

# Giant Second-Order Susceptibility in Monolayer WSe<sub>2</sub> via Strain Engineering

Zhizi Guan<sup>1</sup>, Yunkun Xu<sup>2</sup>, Junwen Li<sup>3</sup>, Hailong Wang<sup>4</sup>, Zhiwei Peng<sup>2</sup>, Dangyuan Lei<sup>2,\*</sup> and David J. Srolovitz<sup>1,†</sup>

<sup>1</sup>*Department of Mechanical Engineering, The University of Hong Kong, Pokfulam Road, Hong Kong SAR*

<sup>2</sup>*Department of Materials Science and Engineering, City University of Hong Kong, Hong Kong SAR*

<sup>3</sup>*DFTWorks LLC, Oakton, VA 22124, USA*

<sup>4</sup>*CAS Key Laboratory of Mechanical Behavior and Design of Materials, Department of Modern Mechanics, University of Science and Technology of China, Hefei, Anhui 230027, China*

Monolayer WSe<sub>2</sub> (ML WSe<sub>2</sub>) exhibits high second harmonic generation (SHG) efficiency under single 1-photon (1-p) or 2-photon (2-p) resonance conditions due to enhanced second-order susceptibility compared with the off-resonance state [1, 2]. Here, we propose a novel strain engineering approach to dramatically boost the in-plane second-order susceptibility ( $\chi_{yyy}$ ) by tuning the biaxial strain to shift two K-valley excitons (the A-exciton and a high-lying exciton (HX)) into double resonance. We first identify the A-exciton and HX from the 2D Mott-Wannier model and compare the enhanced  $\chi_{yyy}$  at single 1-p and 2-p resonance states. The strongest enhancement arises from the 2-p resonance state of HX. By applying a small uniform biaxial strain (0.16%), we observe an excitonic double resonance state ( $E_{HX} = 2E_A$ ,  $E_{HX}$  and  $E_A$  are the exciton absorption energies). Strain-tuning can yield up to a 50X enhancement in  $\chi_{yyy}$  compared to the single 2-p resonance state of HX, resulting in a further three orders of magnitude enhancement in SHG efficiency. Further exploration of strain states near 0.16% reveals double resonance also occurs at other wavevectors near the K valley, leading to a further increase in  $\chi_{yyy}$ , confirming that strain engineering is an effective methodology for enhancing  $\chi_{yyy}$ . Our findings suggest new avenues for strain engineering the optical properties of 2D materials for novel nonlinear optoelectronics applications.

Second harmonic generation (SHG) is a process where incident photons interact with a nonlinear, noncentrosymmetric crystal to generate new photons with twice the initial frequency [3, 4]. SHG finds significant applications in monolayer materials due to their atomic thickness induced phase matching between the incident and second harmonic waves for efficient SHG output, as well as exciton states that can enhance SHG intensity via excitonic resonance [5–10]. An important strategy to enhance the second-order susceptibility ( $\chi^{(2)}$ ) is through one-photon (1-p) or two-photon (2-p) resonance [1, 2, 11–19]; the SHG intensity is proportional to the square of the second-order susceptibility [20]. Achieving these two single resonance states entails the alignment of virtual states with the eigenenergy levels of the material during the SHG process. In monolayer materials, this can be achieved by matching the energy of one (1-p) or two (2-p) incident photons with the exciton energy. Lin et al. [1] reported a narrow and intense SHG peak from a 716 nm continuous-wave (CW) laser resonantly driving the A-exciton in ML WSe<sub>2</sub>. The observation of a strong SHG signal from a low pump irradiance (CW rather than femtosecond laser) provides strong evidence of the 1-p A-exciton resonance inducing a large second-order susceptibility [11]. Wang et al. [2] reported a 2-p resonance state in ML WSe<sub>2</sub> by targeting 2-photon excitation energy at the A-exciton, leading to an up to 3 orders of magnitude enhancement in SHG efficiency (compared with the off-resonance state).

To further enhance the second-order susceptibility, we propose to use a combination of 1-p and 2-p processes at a single

wavevector; i.e. "double resonance" (Fig 1b). Double resonance is a promising approach to inducing a giant enhancement in the second-order susceptibility compared to single 1-p or 2-p resonance state [16, 21–25]. However, to our knowledge, double resonance has never been observed in real experiments due to its restrictive band configuration criteria: three bands must form two continually nested states (in reciprocal space); this is an extension of the two-band nesting concept in first-order linear absorption processes [26–28]. A recent experiment identified a novel bright exciton with an in-plane dipole and negative effective mass, termed the "high-lying exciton" (HX), at the K valley [1]. Remarkably, the energy of the HX is close to twice that of the A-exciton in ML WSe<sub>2</sub>, rendering it an ideal candidate for achieving double resonance combined with the A-exciton.

In this study, we investigate the potential of the high-lying exciton for boosting in-plane second-order susceptibility ( $\chi_{yyy}$ ) through double resonance with A-exciton in ML WSe<sub>2</sub>. We explore the application of biaxial strain ( $\eta$ ) engineering to tune the band energies around the K valley and two exciton states in order to enhance  $\chi_{yyy}$ . First, we identify the exciton binding energy and the absorption peaks ( $E_A$ ,  $E_{HX}$ ) within a 2D Mott-Wannier model and first-principle calculations. We then compare the single 1-p and 2-p resonance state enhanced  $\chi_{yyy}$  and find that the strongest on-resonance  $\chi_{yyy}$  comes from the 2-p resonance state at HX in unstrained ML WSe<sub>2</sub>. By applying a biaxial tensile strain ( $\eta = 0.16\%$ ) to satisfy the excitonic double resonance condition ( $E_{HX} = 2E_A$ ), we observe a  $\sim 50$ -fold enhancement in  $\chi_{yyy}$  compared to the single 2-p resonance at HX, leading to a further three orders of magnitude enhancement in the SHG efficiency. By exploring different strain states to achieve double resonance at other wavevectors near the K valley ( $0.16\% \leq \eta \leq 0.67\%$ ), the

\* dangylei@cityu.edu.hk

† srol@hku.hk

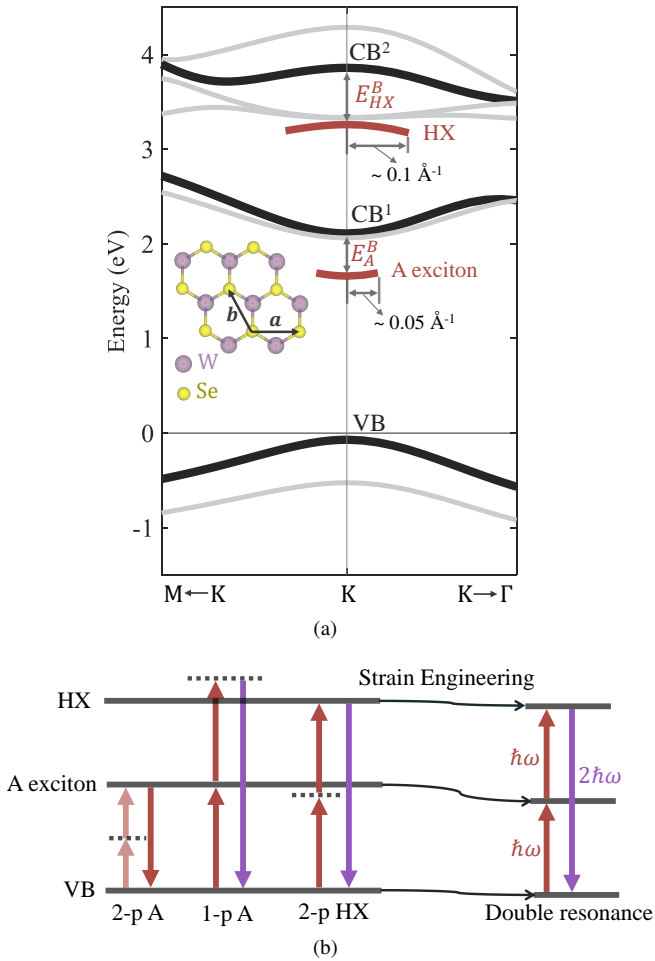


FIG. 1. (a) Crystal structure and band structure (near the K valley) of ML WSe<sub>2</sub>. Three spin-split bands forming the A-exciton (VB, CB<sup>1</sup>) and the HX (VB, CB<sup>2</sup>) are highlighted. We label two exciton binding energies ( $E_A^B$ ,  $E_{HX}^B$ ) according to our 2D Mott-Wannier model calculations. The excitons are labeled based on their envelope functions from reference [1]. (b) A schematic of 1-photon (1-p), 2-photon (2-p), and double resonance states in ML WSe<sub>2</sub> based on A-exciton and HX. The dashed and solid lines depict the SHG virtual states and real exciton states, respectively. Single 1-p or 2-p resonance requires that the incident energy or twice the incident energy meet the excitonic energy, while double resonance occurs when both energy matching requirements are met, which may be manipulated by strain engineering to achieve.

double resonance effect also enhances  $\chi_{yyy}$  compared to the single 1-p or 2-p resonance state. Our findings demonstrate the potential of strain engineering in 2D materials for optimizing optical properties. Materials with strongly enhanced second-order susceptibility hold considerable potential in different nonlinear optoelectronic applications.

We obtain the optimized crystal structures and self-consistent wavefunctions using density functional theory (DFT) within the projected augmented wave (PAW) formalism implemented in VASP [29–31]. We compare the Perdew–Burke–Ernzerhof (PBE) and Heyd–Scuseria–Ernzerhof (HSE) hybrid functionals for describing electron exchange

correlation, with previously reported self-consistent GW results [32, 33]. Our main results are based on the PBE scheme; the PBE and HSE band shapes exhibit negligible difference near the K valley (see Fig. S1), while the choice of PBE effectively reduces the computational demands compared with HSE and GW-based calculations. Neither PBE nor HSE band structures compare well with GW results using only a single-step scissor correction at the band gap. Therefore, we apply different corrections for different conduction band valleys to ensure that the corrected bands align well with the previously reported GW results [1] (scissor correction details and comparisons among exchange-correlation schemes are provided in Sections I and II of the SM).

We determine the second-order susceptibility tensor ( $\chi^{(2)}$ ) within the independent-particle approximation (IPA) while with adequate correction, which well describes our target excitons (A-exciton, HX) for discussion. In addition to the PAW-PBE, we also describe electron and hole wavefunctions using the maximally localized Wannier function (MLWF) basis [34]. Comparisons and computation details may be found in Section IV of the SM. Wannier interpolation is utilized to efficiently compute energy and momentum matrix elements on an arbitrary  $\mathbf{k}$  grid in reciprocal space. It is important to note that achieving double resonance leads to numerical difficulties (divergences) in evaluating the second-order susceptibility using regular Monkhorst-Pack sampling. Hence, we employ a method in which the target Brillouin zone is divided into triangles across which the energy and momentum matrix elements are linear within each triangle [16, 35] to achieve faster convergence and improved accuracy of our second-order susceptibility results (see Section V, Fig. S5, S6 of the SM).

Our first step is to identify the A-exciton and HX based on the scissor-corrected band structure and the Mott-Wannier model. We use the experimentally-defined lattice constant (3.282 Å) in our calculation model for direct comparison with previously reported experimental results. Fig. 1a illustrates the atomic structure and band structure of ML WSe<sub>2</sub>, exhibiting a direct band gap at the K valley of 2.18 eV. We then determine the exciton binding energy using the Mott-Wannier model, regarding the electron-hole pair as a "pseudo-hydrogen atom" [36]. The 3D Mott-Wannier exciton model must be modified to account for the non-local and wavevector-dependent screening in 2D materials. Hence, we employ the 2D Mott-Wannier model [37] to calculate the binding energy as  $E^B = (8\mu)/(1 + \sqrt{1 + 32\pi\alpha\mu/3})^2$ , where  $\mu$  represents the reduced effective mass of the electron-hole pair forming the exciton ( $\mu^{-1} = m_e^{-1} + m_h^{-1}$ ).  $\mu$  can be fit from the band structure as  $\hbar^2(d^2E(\mathbf{k})/d\mathbf{k}^2)^{-1}$ , where  $\hbar$  is the reduced Planck constant and  $E(\mathbf{k})$  is the energy band dispersion in momentum space.  $\alpha$  denotes the internal polarizability, which is linearly fit to the wavevector-dependent dielectric constant.

In ML WSe<sub>2</sub>, the A-exciton and HX can be depicted as an electron and hole in three bands forming two pairs in Fig. 1a (A: VB, CB<sup>1</sup>; HX: VB, CB<sup>2</sup>). Based on the PBE functional results, the A and HX exciton binding energies are 0.48 eV and 0.58 eV in ML WSe<sub>2</sub>, respectively, in good agreement with reported BSE results (A: 0.45 eV, HX: 0.6 eV). Therefore, the absorption energy of A ( $E_A$ ) and HX ( $E_{HX}$ )

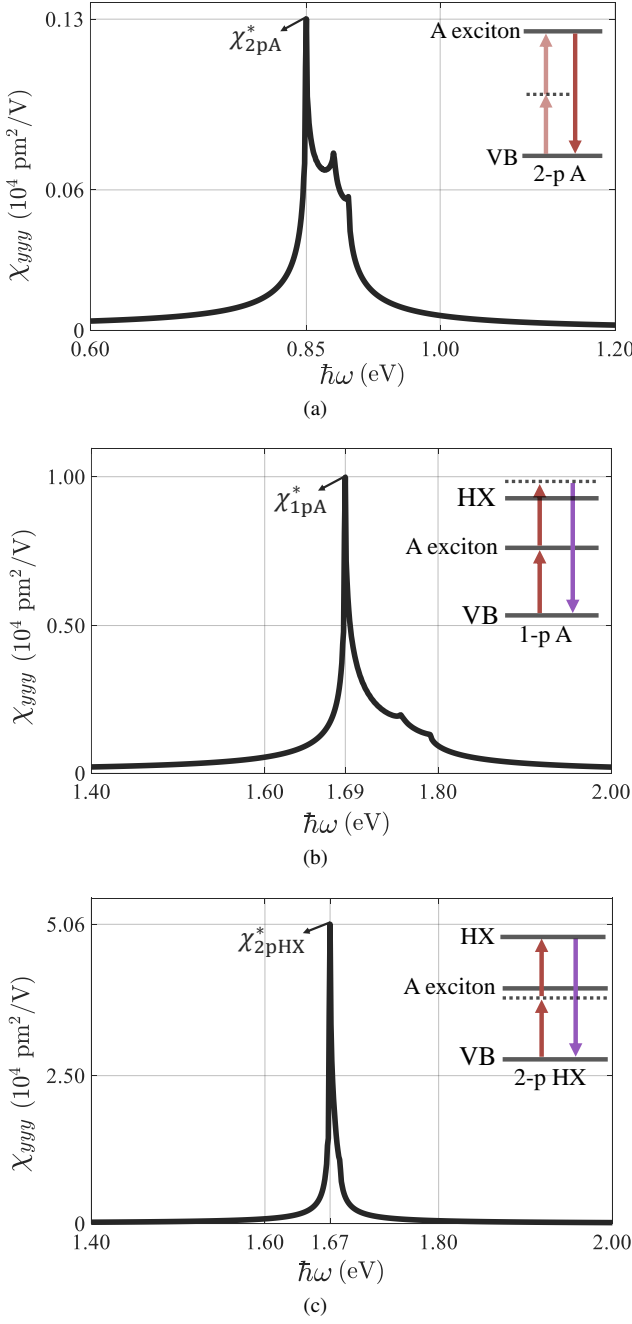


FIG. 2. The absolute value of the in-plane SHG susceptibility  $\chi_{yyy}$  versus incident photon energy  $\hbar\omega$  at the single 1-p or 2-p resonance state - see Fig. 1(b). We label the peak at each on-resonance incident energy as (a)  $\chi_{2pA}^*$ , (b)  $\chi_{1pA}^*$ , and (c)  $\chi_{2pHX}^*$  to compare the enhancement among different states.

in the unstrained ML WSe<sub>2</sub> is at 1.70 eV and 3.35 eV, respectively, by subtracting each binding energy from the GW gap at the K valley. By calculating the oscillator strength ( $|\langle \psi_v | \hat{p} | \psi_c \rangle|^2 / (E_c - E_v)$ ,  $v \in \{VB\}$ ,  $c \in \{CB^1, CB^2\}$ ) at the K valley for the two excitons in Fig. S9 (c), we found that the oscillator strength ratio also correspond with previous BSE results (i.e., the intensity ratio HX: A  $\approx$  1:18), but

at much lower computational cost [1] (Section III of the SM). In summary, our PBE-based description of two excitons, with appropriate corrections, enables a good representation of the A-exciton and HX for subsequent strain engineering.

Based on the identification of two excitons, we explore how single 1-p and 2-p resonance from the A-exciton and HX enhances  $\chi_{yyy}$ . Fig. S7 shows the  $\chi_{yyy}$  spectrum when the incident photon energy  $\hbar\omega$  ranges from 0.5-4 eV, covering the energies from half the A-exciton energy to the HX. The four peaks on the spectrum (from low to high energy) correspond to the 2-p A, 2-p HX, 1-p A, and 1-p HX on-resonance state-induced  $\chi_{yyy}$  enhancement. Due to the relatively small value of the 1-p HX peak and its uV emission energy, we focus on the first three resonance states. Fig. 2(a)-(c) separately shows three single resonance effects near the resonance incident energy, and we label the highest on-resonance  $\chi_{yyy}$  peak as  $\chi^*$  to observe the maximum enhancement fold (we isolated the 1-p and 2-p states in the  $\chi_{yyy}$  calculation - see Section V, SM).

Fig. 2(a) shows as an example describing the 2-p A resonance. We clearly observe that  $\chi_{yyy}$  is 30-40X that of the off-resonance state susceptibility at  $\hbar\omega = 0.85$  eV (i.e.,  $\chi_{2pA}^*$ ), in agreement with the previous report 3 orders of magnitude enhancement of the SHG efficiency from 2-p A resonance [2]. Among the three enhancement states, the strongest comes from 2-p HX resonance; this is likely because the intermediate virtual state energy is nearly aligned with the A-exciton energy, leading to a state that is closest to double resonance amongst the three. Hence, we use the 2-p HX resonance result to benchmark the double resonance enhancement effect in the next step.

We then proposed to tune the energies of the A-exciton and HX into excitonic double resonance; i.e., to ensure that  $E_{HX} = 2E_A$  where  $E_{HX}$  and  $E_A$  are the absorbance energies for these two excitons. Without external tuning,  $E_{HX} < 2E_A$  in ML WSe<sub>2</sub>. We tune these energy levels via strain engineering (via easy to implement biaxial strain) to shift the bands relative to the Fermi level and the excitonic levels relative to each other [38]. Fig. 3(a) shows how  $E_A$  and  $E_{HX}$  respond to strain ( $\eta$ ,  $-1\% \leq \eta \leq 1\%$ ) in ML WSe<sub>2</sub>. They both redshift with increasing  $\eta$ , consistent with experimental reports [39, 40]. To interpret the variation trend, we examine the effect of strain  $\eta$  on the VB, CB<sup>1</sup> and CB<sup>2</sup> band energies ( $E_v^o$ ,  $E_{c1}^o$ ,  $E_{c2}^o$ ) and the exciton binding energies ( $E_A^B$ ,  $E_{HX}^B$ ) at the K valley (Fig. S9). The relative shift rate between the CB<sup>1</sup> and VB is almost four times larger than that between CB<sup>2</sup> and VB due to different bonding nature in different bands (Fig. S10). And the A and HX exciton binding energy  $E^B$  decreases with increasing  $\eta$ . This may be attributed to more spatially separated electron-hole pairs, with weaker Coulomb interactions, with increasing  $\eta$ .

Fig. 3(a) illustrates the relationship between  $E_A(\eta)$  and  $E_{HX}(\eta)$  as well as the excitonic double resonance condition ( $E_{HX} = 2E_A$ ). This condition is satisfied at  $\eta = 0.16\%$ , where  $E_A = 1.67$  eV and  $E_{HX} = 3.34$  eV. By calculating the relative enhancement  $\chi_{yyy}/\chi_{2pHX}^*$  under the double resonance condition, we see (Fig. 3b) that this strain leads to an up to  $\sim 50X$  enhancement in  $\chi_{yyy}$  compared with the single 2-p HX resonance result in unstrained ML WSe<sub>2</sub>. This  $\sim 50X$

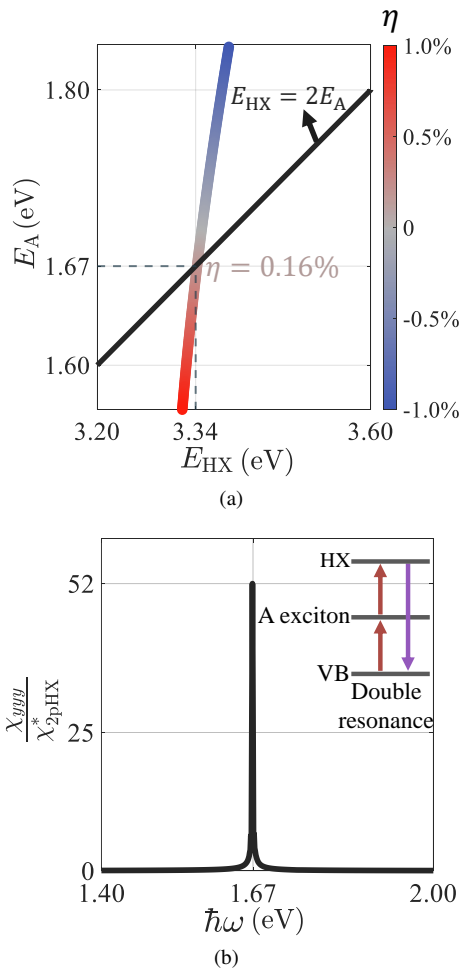


FIG. 3. (a) The relationship between the exciton energies of the  $E_{\text{HX}}$  and  $E_{\text{A}}$  as a function of biaxial strain,  $\eta$  (colored line; the color bar on the right is strain,  $\eta$ ). The dark line illustrates the double resonance condition,  $E_{\text{HX}} = 2E_{\text{A}}$ . The crossing of the dark and colored line indicates that double resonance in ML WSe<sub>2</sub> occurs at  $\eta = 0.16\%$ . (b) The in-plane SHG susceptibility,  $\chi_{yyy}$ , as a function of incident photon energy at double resonance ( $\eta = 0.16\%$ ). The y-axis, labeled  $\chi_{yyy}/\chi_{2\text{pHX}}^*$ , shows an  $\sim 50\text{X}$  enhancement appears at the double resonance on-resonance incident energy  $\sim 1.67\text{ eV}$ .

enhancement in  $\chi_{yyy}$  can produce a 3-order of magnitude increase in the in-plane SHG intensity based on the single 1-p or 2-p resonance result via easy-to-implement biaxial strain engineering, making ML WSe<sub>2</sub> considerably potent for many nonlinear optoelectronic applications.

The 50-fold enhancement in  $\chi_{yyy}$  (based on single 2-p HX resonance) is an important tuning outcome. More enhancement is possible through tuning based on the excitonic energy over the entire exciton band, as other double resonance states are possible in addition to the K valley. Hence we first examine other strain state-induced  $\chi_{yyy}$  enhancement - see Fig. 4(a). The strongest enhancement appears near  $\hbar\omega = 1.67\text{ eV}$ ; i.e., the K-valley double resonance energy. Besides the strongest enhancement at  $\eta = 0.16\%$ , other strains lead to an enhancement of  $\chi_{yyy}$  relative to the single on res-

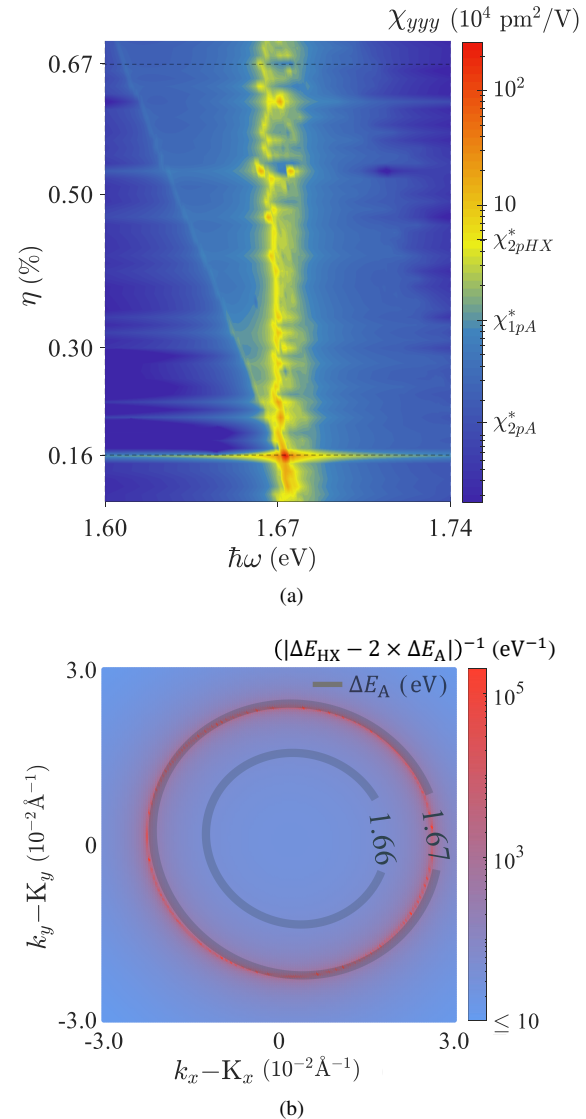


FIG. 4. (a) The absolute value of  $\chi_{yyy}$  versus the biaxial strain  $\eta$  in the range where double resonance can occur near the K valley (in the DFT predicted range,  $0.16\% \leq \eta \leq 0.67\%$ ). Three on-resonance enhancements from single 1-p and 2-p resonance are labeled in the colorbar for easy comparison. (b) The double resonance condition  $|\Delta E_{\text{HX}} - 2\Delta E_{\text{A}}|^{-1}$  for one biaxial strain  $\eta = 0.32\%$  ( $\Delta E_{\text{A}} = E_{c1}^o - E_v^o - E_{\text{A}}^B$ ;  $\Delta E_{\text{HX}} = E_{c2}^o - E_v^o - E_{\text{HX}}^B$ ). The overlap between the  $\Delta E_{\text{A}} = 1.67\text{ eV}$  (gray) contour and the region where  $|\Delta E_{\text{HX}} - 2\Delta E_{\text{A}}|^{-1}$  is large shows the double resonance effect beyond the K valley.

onance  $\chi_{yyy}$  (i.e.,  $\chi_{2\text{pHX}}^*$ ,  $\chi_{1\text{pA}}^*$ , and  $\chi_{2\text{pA}}^*$ ) in the unstrained monolayer. Fig. 4(a) demonstrates that strain tuning is an effective approach for enhancing the second-order susceptibility compared to previously reported single 1-p and 2-p resonance methodologies.

To explain the strain tuning effects outside of the K valley, we explore the exciton energy (from our band diagrams) and the binding energy. Fig. S13 shows contours of the energies for the A-exciton ( $\Delta E_{\text{A}} = E_{c1}^o - E_v^o - E_{\text{A}}^B$ ) and HX ( $\Delta E_{\text{HX}} = E_{c2}^o - E_v^o - E_{\text{HX}}^B$ ) in  $k_x - k_y$  near the K valley in ML WSe<sub>2</sub>. We

quantify the A-exciton energy  $\Delta E_A(\mathbf{k}, \eta)$  by fitting the 2D  $E\text{-}\mathbf{k}$  diagram to a circle as  $\Delta E_A(\mathbf{k}, \eta) = \Delta E_A(K, \eta) + (\hbar^2/2m_{c1}(\eta) - \hbar^2/2m_v(\eta))(k_x^2 + k_y^2)$ , where  $m_{c1}$  and  $m_v$  are the CB<sup>1</sup> and VB effective masses in the K valley (Fig. S11, S12).  $\Delta E_{\text{HX}}$  exhibits a much smaller variation ratio (with larger anisotropy) than  $\Delta E_A$  (Fig. 3b). Hence, we approximate  $\Delta E_{\text{HX}}(\mathbf{k}, \eta) = \Delta E_{\text{HX}}(K, \eta)$ , where  $\Delta E_{\text{HX}}(K, \eta)$  is the HX band energy difference in the K valley.

To achieve double resonance,  $\Delta E_{\text{HX}}(\mathbf{k}, \eta) = 2\Delta E_A(\mathbf{k}, \eta)$  must have a solution  $\eta(\mathbf{k})$  in  $\sqrt{k_x^2 + k_y^2} \leq 5 \times 10^{-2} \text{ \AA}^{-1}$  (where both excitonic envelope functions are greater than 0). This occurs for  $0.16\% \leq \eta \leq 0.67\%$  (dashed lines in Fig. 4a). At  $\eta = 0.16\%$ , only the K-valley wavevector satisfies the double resonance condition, leading to the strongest enhancement in  $\chi_{yyy}$ . As  $\eta$  increases from 0.16%, the double resonance condition is met at other wavevectors, forming a circle of wavevectors satisfying double resonance. At  $\eta = 0.67\%$ , the double resonance wavevector circle reaches the edges of the A-exciton range. We illustrate this by plotting the energy of  $|\Delta E_{\text{HX}} - 2\Delta E_A|^{-1}$  and the  $\Delta E_A$  contour versus  $\mathbf{k}$  on the same figure, in Fig. 4b (for  $\eta = 0.32\%$ ). We observe a circle of overlapping states around the K valley;  $|\Delta E_{\text{HX}} - 2\Delta E_A|^{-1}$  is a maximum (red) and overlaps the  $\Delta E_A = 1.67 \text{ eV}$  contour. This proves the existence of double resonance near the K valley, corresponding with the  $\chi_{yyy}$  result in Fig. 4a and Fig. S8 for the 2X enhancement of  $\chi_{yyy}$  peak intensity (compared with  $\chi_{2p\text{HX}}^*$  of the unstrained monolayer) for an incident photon energy of 1.67 eV.

Our first-principle calculations indicate that a small strain can produce a very large enhancement of the second-order susceptibility and the corresponding SHG output, reminiscent of previous experiments. We find that different experimental measurements of second-order susceptibility in ML WSe<sub>2</sub> yield very different results (up to two-orders of magnitude) [19, 41, 42]. We speculate that this difference may arise from the strain-induced double resonance effect when ML WSe<sub>2</sub> is placed on a substrate for SHG measurements. Rahman et al.

[43] estimated that a 0.35% strain was presented in a wrinkled monolayer of CuInP<sub>2</sub>S<sub>6</sub> (CIPS) and showed that this led to an 160-fold increase in the SHG intensity (which was sensitive to incident photon energy). Their experimental observation of a giant SHG enhancement may indeed be the result of the excitonic double resonance mechanism suggested here. This provides further impetus for further experiments as a function of strain (and possibly strain gradients) to engineer the second-order susceptibility.

In conclusion, we explored the potential of exploiting high-lying exciton double resonance (with the A-exciton) to induce a giant enhancement ( $\sim 50$ -fold) in second-order susceptibility ( $\chi_{yyy}$ ) of ML WSe<sub>2</sub>. We further demonstrated that biaxial strain is an effective approach to tune the band energies and excitonic states into double resonance. We identify two excitonic absorbance peaks ( $E_A, E_{\text{HX}}$ ) and their binding energies ( $E^B$ ) within the 2D Mott-Wannier model. Our results exhibit good agreement with those from previous Bethe-Salpeter equation BSE results (with much lower computational demands) and experiments. Comparing the 1-p and 2-p resonance state enhanced  $\chi_{yyy}$  in the unstrained ML WSe<sub>2</sub> shows that the strongest enhancement arises from the 2-p resonance state of HX. Subsequently, we strain-tune the excitonic absorption energy relationship to achieve double resonance ( $E_{\text{HX}} = 2E_A$ ). A tensile biaxial strain of 0.16% leads to a maximum (50X enhancement) in  $\chi_{yyy}$  compared with the on-resonance 2-p HX result of the unstrained monolayer. Further exploration of the effect of strain reveals the existence of other double resonance states near the K valley that also enhance  $\chi_{yyy}$ . Overall, our results suggest new possibilities for strain-tuning 2D material properties to greatly enhance optoelectronic properties for novel potential future optoelectronic applications.

Acknowledgment - The authors acknowledge the financial support by the Research Grants Council of Hong Kong (YX, ZP, and DL- GRF Grant No. 15304519, DJS and ZG - GRF Grant No. 11211019), and support from the National Natural Science Foundation of China (HW - Grants No. 12172347 and No. 12232016).

---

[1] K.-Q. Lin, C. S. Ong, S. Bange, P. Faria Junior, B. Peng, J. Ziegler, J. Zipfel, C. Bäuml, N. Paradiso, K. Watanabe, T. Taniguchi, C. Strunk, B. Monserrat, J. Fabian, A. Chernikov, D. Qiu, S. Louie, and J. Lupton, Narrow-band high-lying excitons with negative-mass electrons in monolayer wse2, *Nature communications* **12**, 5500 (2021).

[2] G. Wang, X. Marie, I. Gerber, T. Amand, D. Lagarde, L. Bouet, M. Vidal, A. Balocchi, and B. Urbaszek, Giant enhancement of the optical second-harmonic emission of wse 2 monolayers by laser excitation at exciton resonances, *Physical review letters* **114**, 097403 (2015).

[3] P. Franken, A. E. Hill, C. e. Peters, and G. Weinreich, Generation of optical harmonics, *Physical Review Letters* **7**, 118 (1961).

[4] J. Zhang, W. Zhao, P. Yu, G. Yang, and Z. Liu, Second harmonic generation in 2d layered materials, *2D Materials* **7**, 042002 (2020).

[5] Y. Wang, S. Das, F. Iyikanat, Y. Dai, S. Li, X. Guo, X. Yang, J. Cheng, X. Hu, M. Ghotbi, F. Ye, H. Lipsanen, S. Wu, T. Hasan, X. Gan, K. Liu, D. Sun, Q. Dai, F. J. García de Abajo, J. Zhao, and Z. Sun, Giant all-optical modulation of second-harmonic generation mediated by dark excitons, *ACS Photonics* **8**, 2320 (2021).

[6] A. Autere, H. Jussila, Y. Dai, Y. Wang, H. Lipsanen, and Z. Sun, Nonlinear optics with 2d layered materials, *Advanced Materials* **30**, 1705963 (2018).

[7] R. W. Boyd, *Nonlinear optics* (Academic press, 2020).

[8] A. R. Khan, L. Zhang, K. Ishfaq, A. Ikram, T. Yildrim, B. Liu, S. Rahman, and Y. Lu, Optical harmonic generation in 2d materials, *Advanced Functional Materials* **32**, 2105259 (2022).

[9] Z. Xie, T. Zhao, X. Yu, and J. Wang, Nonlinear optical properties of 2d materials and their applications, *Small* , 2311621 (2024).

[10] A. Ciattoni, A. Marini, C. Rizza, and C. Conti, Phase-matching-

free parametric oscillators based on two-dimensional semiconductors, *Light: Science & Applications* **7**, 5 (2018).

[11] K. Yao, E. Yanev, H. J. Chuang, M. R. Rosenberger, X. Xu, T. Darlington, K. M. McCreary, A. T. Hanbicki, K. Watanabe, T. Taniguchi, B. T. Jonker, X. Zhu, D. N. Basov, J. C. Hone, and P. J. Schuck, Continuous wave sum frequency generation and imaging of monolayer and heterobilayer two-dimensional semiconductors, *ACS Nano* **14**, 708 (2020).

[12] Y. Song, R. Tian, J. Yang, R. Yin, J. Zhao, and X. Gan, Second harmonic generation in atomically thin m<sub>2</sub>e<sub>2</sub>, *Advanced Optical Materials* **6**, 1701334 (2018).

[13] L. Tam, D. Clark, F. Ullah, J. Jang, S. Velusamy, Y. Sim, M.-J. Seong, K.-H. Chung, J. Kim, S. Park, S. H. Rhim, G. Kim, and Y. s. Kim, Impact of selenium doping on resonant second-harmonic generation in monolayer mos<sub>2</sub>, *Acs Photonics* **4**, 38 (2017).

[14] F. Yang, W. Song, F. Meng, F. Luo, S. Lou, S. Lin, Z. Gong, J. Cao, E. S. Barnard, E. Chan, L. Yang, and J. Yao, Tunable second harmonic generation in twisted bilayer graphene, *Matter* **3**, 1361 (2020).

[15] Y. Shan, Y. Li, D. Huang, Q. Tong, W. Yao, W.-T. Liu, and S. Wu, Stacking symmetry governed second harmonic generation in graphene trilayers, *Science advances* **4**, eaat0074 (2018).

[16] S. J. Brun and T. G. Pedersen, Intense and tunable second-harmonic generation in biased bilayer graphene, *Physical Review B* **91**, 205405 (2015).

[17] S. Shree, D. Lagarde, L. Lombez, C. Robert, A. Balocchi, K. Watanabe, T. Taniguchi, X. Marie, I. Gerber, M. Glazov, L. Golub, B. Urbaszek, and I. Paradiso, Interlayer exciton mediated second harmonic generation in bilayer mos<sub>2</sub>, *Nature Communications* **12**, 1 (2021).

[18] Y. Dai, Y. Wang, S. Das, H. Xue, X. Bai, E. Hulkko, G. Zhang, X. Yang, Q. Dai, and Z. Sun, Electrical control of interband resonant nonlinear optics in monolayer mos<sub>2</sub>, *ACS nano* **14**, 8442 (2020).

[19] K. L. Seyler, J. R. Schaibley, P. Gong, P. Rivera, A. M. Jones, S. Wu, J. Yan, D. G. Mandrus, W. Yao, and X. Xu, Electrical control of second-harmonic generation in a wse<sub>2</sub> monolayer transistor, *Nature nanotechnology* **10**, 407 (2015).

[20] Z. Guan, Y. Xu, J. Li, H. Wang, Z. Peng, D. Lei, and D. J. Srolovitz, Electric field induced out-of-plane second-order optical nonlinearity in monolayer transition metal dichalcogenides, *Phys. Rev. B* **109**, 075417 (2024).

[21] C.-g. Duan, J. Li, Z.-q. Gu, and D.-s. Wang, First-principles calculation of the second-harmonic-generation coefficients of borate crystals, *Physical Review B* **60**, 9435 (1999).

[22] J. Sipe and A. Shkrebtii, Second-order optical response in semiconductors, *Physical Review B* **61**, 5337 (2000).

[23] J. Cabellos, B. S. Mendoza, M. Escobar, F. Nastos, and J. Sipe, Effects of nonlocality on second-harmonic generation in bulk semiconductors, *Physical Review B* **80**, 155205 (2009).

[24] M. L. Trolle, G. Seifert, and T. G. Pedersen, Theory of excitonic second-harmonic generation in monolayer mos<sub>2</sub>, *Physical Review B* **89**, 235410 (2014).

[25] S. R. Biswas, J. Yu, Z. Wang, D. R. da Costa, C. Zhao, S. Yuan, and T. Low, Double resonant tunable second harmonic generation in two-dimensional layered materials through band nesting, *Physical Review B* **107**, 115409 (2023).

[26] F. Bassani, G. P. Parravicini, R. A. Ballinger, and J. L. Birman, Electronic states and optical transitions in solids (1976).

[27] A. Carvalho, R. Ribeiro, and A. C. Neto, Band nesting and the optical response of two-dimensional semiconducting transition metal dichalcogenides, *Physical Review B* **88**, 115205 (2013).

[28] L. Mennel, V. Smejkal, L. Linhart, J. Burgdorfer, F. Libisch, and T. Mueller, Band nesting in two-dimensional crystals: An exceptionally sensitive probe of strain, *Nano letters* **20**, 4242 (2020).

[29] G. Kresse and J. Furthmüller, Efficient iterative schemes for ab initio total-energy calculations using a plane-wave basis set, *Phys. Rev. B* **54**, 11169 (1996).

[30] J. P. Perdew, K. Burke, and M. Ernzerhof, Generalized gradient approximation made simple, *Phys. Rev. Lett.* **77**, 3865 (1996).

[31] P. E. Blöchl, Projector augmented-wave method, *Phys. Rev. B* **50**, 17953 (1994).

[32] J. Heyd, G. E. Scuseria, and M. Ernzerhof, Hybrid functionals based on a screened coulomb potential, *The Journal of chemical physics* **118**, 8207 (2003).

[33] J. Heyd and G. E. Scuseria, Efficient hybrid density functional calculations in solids: Assessment of the heyd–scuseria–ernzerhof screened coulomb hybrid functional, *The Journal of chemical physics* **121**, 1187 (2004).

[34] A. A. Mostofi, J. R. Yates, Y.-S. Lee, I. Souza, D. Vanderbilt, and N. Marzari, wannier90: A tool for obtaining maximally-localised wannier functions, *Computer physics communications* **178**, 685 (2008).

[35] G. Wiesenecker, G. Te Velde, and E. Baerends, Analytic quadratic integration over the two-dimensional brillouin zone, *Journal of Physics C: Solid State Physics* **21**, 4263 (1988).

[36] G. H. Wannier, The structure of electronic excitation levels in insulating crystals, *Physical Review* **52**, 191 (1937).

[37] T. Olsen, S. Latini, F. Rasmussen, and K. S. Thygesen, Simple screened hydrogen model of excitons in two-dimensional materials, *Physical review letters* **116**, 056401 (2016).

[38] Z. Guan, W. Yang, H. Wang, H. Wang, and J. Li, Direct band gap and anisotropic transport of znsb monolayers tuned by hydrogenation and strain, *RSC advances* **12**, 2693 (2022).

[39] B. Aslan, M. Deng, and T. F. Heinz, Strain tuning of excitons in monolayer wse<sub>2</sub>, *Physical Review B* **98**, 115308 (2018).

[40] Z. Peng, X. Chen, Y. Fan, D. J. Srolovitz, and D. Lei, Strain engineering of 2d semiconductors and graphene: from strain fields to band-structure tuning and photonic applications, *Light: Science & Applications* **9**, 190 (2020).

[41] J. Ribeiro-Soares, C. Janisch, Z. Liu, A. Elías, M. Dresselhaus, M. Terrones, L. Cançado, and A. Jorio, Second harmonic generation in wse<sub>2</sub>, *2D Materials* **2**, 045015 (2015).

[42] H. G. Rosa, Y. W. Ho, I. Verzhbitskiy, M. J. Rodrigues, T. Taniguchi, K. Watanabe, G. Eda, V. M. Pereira, and J. C. Gomes, Characterization of the second-and third-harmonic optical susceptibilities of atomically thin tungsten diselenide, *Scientific reports* **8**, 10035 (2018).

[43] S. Rahman, T. Yildirim, M. Tebyetekerwa, A. R. Khan, and Y. Lu, Extraordinary nonlinear optical interaction from strained nanostructures in van der waals cuinp2s6, *ACS nano* **16**, 13959 (2022).